

Federated-inspired Single-cell Batch Integration in Latent Space

Quang-Huy Nguyen¹ Zongliang Yue² Hao Chen³ Wei-Shinn Ku¹ Jiaqi Wang¹

¹Department of Computer Science and Software Engineering, Auburn University

²Harrison College of Pharmacy, Auburn University

³College of Forestry, Wildlife and Environment, Auburn University

Abstract

Advances in single-cell RNA sequencing enable the rapid generation of massive, high-dimensional datasets, yet the accumulation of data across experiments introduces batch effects that obscure true biological signals. Existing batch correction approaches either insufficiently correct batch effects or require centralized retraining on the complete dataset, limiting their applicability in distributed and continually evolving single-cell data settings. We introduce `scBatchProx`, a post-hoc optimization method inspired by federated learning principles for refining cell-level embeddings produced by arbitrary upstream methods. Treating each batch as a client, `scBatchProx` learns batch-conditioned adapters under proximal regularization, correcting batch structure directly in latent space without requiring raw expression data or centralized optimization. The method is lightweight and deployable, optimizing batch-specific adapter parameters only. Extensive experiments show that `scBatchProx` consistently yields relative gains of approximately 3–8% in overall embedding quality, with batch correction and biological conservation improving in 90% and 85% of data–method pairs, respectively. We envision this work as a step toward the practical refinement of learned representations in dynamic single-cell data systems.

1 Introduction

Advances in single-cell RNA sequencing (scRNA-seq) technologies now enable the profiling of thousands to millions of cells in a single experiment [4, 8, 15, 2], driving an unprecedented growth of single-cell gene expression data. This expansion is evident in public repositories: as of November 2025, CELLxGENE hosts 139.8 million cells spanning more than 1,000 annotated cell types [13], while the Human Cell

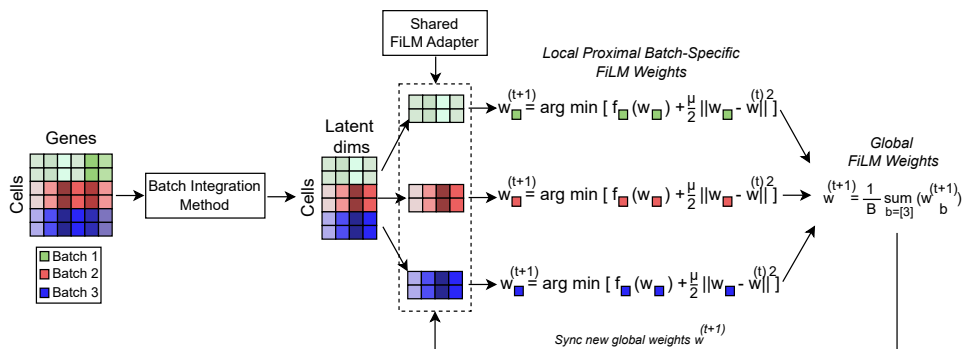


Figure 1: Framework of `scBatchProx`.

Atlas portal reports 63.3 million cells [14]. However, as data accumulate across experiments, platforms, and laboratories, technical variation between batches becomes increasingly pronounced. These batch effects can dominate learned representations, confounding downstream analyses and obscuring true biological signals.

Many existing methods have been proposed to mitigate batch effects; however, they face a fundamental trade-off: some inadequately correct batch effects, while others achieve strong correction only under assumptions that rarely hold in practice (see Section 2). In particular, methods that rely on centralized retraining struggle in dynamic settings where embeddings are produced once and reused, data are distributed across sites, or new studies arrive continually over time. In such settings, repeatedly retraining end-to-end models is not only computationally expensive but also fundamentally mismatched to how scRNA-seq data are generated and reused.

Federated learning (FL) [10] is a decentralized learning paradigm in which multiple clients collaboratively train a global model without the need to share their data. Beyond its systems-level motivation, a key strength of FL lies in its ability to coordinate learning across heterogeneous participants, each characterized by distinct data distributions and local structure, while maintaining global consistency. This setting closely mirrors the challenges posed by batch effects in scRNA-seq data, where experiments differ in technical characteristics yet share underlying biological signals. Moreover, FL naturally supports incremental participation, allowing new clients to contribute updates without requiring centralized access to all historical data. From this perspective, single-cell batch integration can be viewed through an FL-inspired lens, in which each batch acts as an independent optimization unit that contributes to a shared representation while preserving its local characteristics.

Model Overview. Here, we study the problem of improving batch-effect correction while simultaneously enabling efficient adaptation in dynamic single-cell settings. We introduce `scBatchProx`, the first post-hoc optimization framework

for single-cell batch-effect removal that operates on precomputed latent embeddings under a FL-driven formulation. As illustrated in Figure 1, `scBatchProx` takes as input a global cell-level embedding matrix produced by an arbitrary upstream batch correction or representation learning method, with cells partitioned by batch or by dataset from the same tissue. Each batch or dataset is treated as a decentralized client, as in a FL system. A shared Feature-wise Linear Modulation (FiLM) adapter [12] with batch-indexed parameters is used to modulate latent representations, and each client locally updates its corresponding FiLM parameters using only its own embeddings. Local optimization is performed under a FedProx objective [5], which penalizes deviations from the current global adapter and stabilizes training under heterogeneous client distributions. After local updates, FiLM parameters are aggregated across clients using federated averaging, inspired by FedAvg [10]. Finally, the updated global FiLM is broadcast back to all clients for the next round. By iteratively alternating between client-side proximal updates and global aggregation, `scBatchProx` learns batch-specific adaptations that effectively mitigate batch effects while preserving shared biological structure, without requiring centralized retraining.

Contributions. We make the following contributions:

- **Post-hoc refinement of precomputed embeddings under a FL-driven formulation.** We conceptualize batch integration as a federated optimization problem over precomputed cell-level embeddings, in which each batch or study is treated as an independent client. `scBatchProx` learns batch-conditioned latent adaptations via a shared FiLM-style adapter optimized under proximal regularization, enabling effective batch alignment without access to raw data or centralized retraining.
- **Lightweight and deployable integration layer.** `scBatchProx` operates as a post-processing step that can be applied to embeddings produced by arbitrary upstream methods. Since only batch-indexed FiLM parameters are optimized, the method is computationally efficient, deployable on CPU, and compatible with existing single-cell analysis pipelines.
- **Flexible post-hoc embedding refinement under dataset evolution.**

`scBatchProx` is designed to improve cell-level embeddings in practical data settings where datasets evolve over time. We show that `scBatchProx` can be applied in both *cumulative retraining* scenarios, where embeddings are periodically recomputed on all available data (i.e., retraining the upstream model on the combined set of existing and newly arrived data), and *continual training* scenarios, where new datasets are incrementally integrated into a fixed reference embedding (i.e., fitting the pretrained upstream model

only on newly arriving data). Figure 2 illustrates these two dataset evolution scenarios. `scBatchProx` supports both cumulative retraining and continual training by refining embeddings post hoc, either after recomputation of all embeddings or by aligning newly arriving embeddings to a fixed reference.

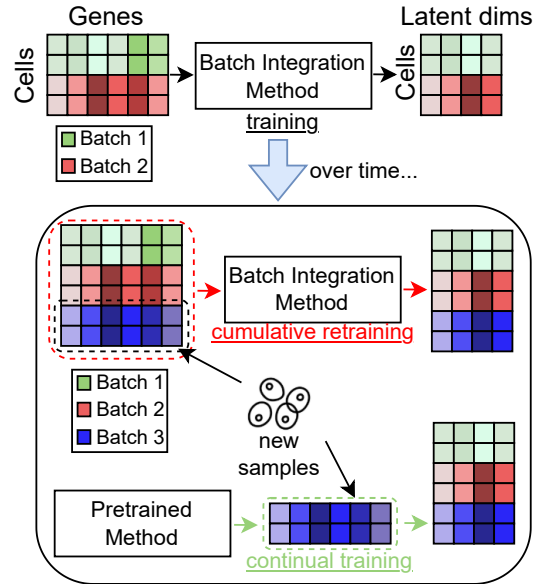


Figure 2: Two dataset evolution scenarios in single-cell analysis. Cumulative retraining recomputes embeddings by retraining the upstream model on all available data, whereas continual training fits newly arriving datasets into a fixed reference embedding without retraining on previously processed data.

2 Related Works

Batch-agnostic Linear Representation Methods. Batch-agnostic linear methods learn low-dimensional representations from high-dimensional gene expression data without incorporating batch information and are commonly used as preprocessing steps in single-cell analysis. Principal component analysis (PCA) identifies orthogonal directions of maximal variance, yielding compact representations that capture dominant sources of variability. Independent component analysis (ICA) seeks statistically independent components and can disentangle mixed signals under assumptions of non-Gaussianity. Factor analysis (FA) models observations using a small number of latent factors with explicit noise modeling, providing a proba-

bilistic interpretation of linear structure. Despite their simplicity, scalability, and interpretability, these approaches are not designed to address batch effects for two prevalent reasons:

First, by ignoring batch identity during representation learning, batch-agnostic linear methods cannot distinguish batch-specific technical variation from biological signal. This limitation becomes particularly severe when batches differ substantially in protocol or exhibit imbalanced cell-type compositions, causing technical effects to be absorbed into the learned components. As a result, the resulting embeddings are often inadequate for robust cross-batch or cross-study integration and require additional downstream correction. `scBatchProx` mitigates this issue by learning batch-conditioned post-hoc corrections in latent space. Specifically, each batch is assigned its own FiLM adapter that models and removes batch-specific shifts on top of a precomputed embedding, without retraining the upstream representation or accessing raw gene expression data.

Second, batch-agnostic methods implicitly assume that a single global linear transformation is sufficient to map all cells from all batches into a shared low-dimensional space. In practice, this forces one global map to simultaneously explain both biological variation and batch-specific differences, even though these differences often require slightly different transformations for different batches. As batch heterogeneity increases, this assumption becomes restrictive and can distort biologically meaningful structure. `scBatchProx` alleviates this constraint by retaining the learned global coordinate system from the upstream method, while allowing each batch to apply a small, batch-specific adjustment in latent space. Importantly, these adjustments are learned so that batch-specific corrections improve alignment without drifting in incompatible directions across batches, preserving biologically shared structure.

Batch-aware Integration and Representation Learning. A substantial body of work addresses batch effects by explicitly incorporating batch information during representation learning. Variational autoencoder based methods learn batch-corrected latent spaces by conditioning the generative process on batch labels, including `scVI` [6], `scANVI` [21], and `LDVAE` [17]. These models operate directly on raw gene expression counts and aim to disentangle biological variation from technical effects through joint probabilistic modeling. When raw data and batch annotations are centrally available, such approaches often achieve strong integration performance and have become widely adopted in single-cell analysis. However, these methods exhibit several technical and operational limitations:

First, batch-aware representation learning methods require direct access to raw gene expression data during training. This requirement limits their applicability in settings where raw data cannot be shared, stored, or reprocessed, for example due to privacy constraints or when embeddings have already been computed and

distributed. In practice, data holders (e.g., laboratories or hospitals) may be unwilling or unable to share raw expression data due to privacy, policy, or logistical constraints. In contrast, `scBatchProx` operates directly on precomputed embeddings and performs batch correction post hoc, allowing representations learned by arbitrary upstream methods to be refined without access to raw gene expression data. `scBatchProx`, thus, avoids the stronger assumption that raw data must remain centrally available throughout training.

Second, batch-aware methods tightly couple batch correction with representation learning, implicitly assuming that batch effects must be addressed at training time. As a result, once embeddings are learned, they are difficult to modify or reuse: integrating new batches typically requires retraining the entire model on all available data. This coupling becomes restrictive in evolving datasets where new experiments arrive over time. `scBatchProx` addresses this limitation by decoupling batch correction from representation learning. By refining embeddings post hoc, `scBatchProx` allows new batches to be integrated through lightweight optimization without retraining the upstream model or revisiting previously processed data.

Third, batch-aware methods require all batches to be trained together in a single centralized procedure, which is impractical when datasets are generated and processed independently across different labs and timelines. In such settings, laboratories must coordinate retraining schedules, previously processed data must be revisited, and models often need to be retrained from scratch whenever new batches arrive, tightly coupling otherwise independent analysis pipelines. `scBatchProx` instead adopts a FL-driven formulation in which each batch is treated as an independent optimization unit. Batch-specific refinements are learned locally and coordinated through a shared latent reference, enabling decentralized and incremental integration workflows while preserving structure that is shared across batches.

3 Methodology

Given a precomputed cell-level embedding produced by an arbitrary upstream method, `scBatchProx` learns batch-conditioned adaptation parameters to reduce batch effects while preserving shared biological structure.

3.1 Problem Setup and Federated Formulation

Let $Z \in \mathbb{R}^{N \times d}$ denote a learned latent embedding matrix for N cells with latent dimension d , and let $b_i \in \{1, \dots, B\}$ denote the batch label for cell i . Each batch

corresponds to a federated client and has access only to its own subset

$$Z_b = \{z_i \mid b_i = b\}.$$

No raw gene expression data are required, and embeddings are never updated during training. Throughout optimization, the latent embeddings Z are treated as fixed inputs, and only batch-conditioned adapter parameters are learned.

Our goal is to learn a batch correction function that maps each embedding z to a batch aligned representation \tilde{z} , while allowing decentralized optimization across batches with limited coordination.

3.2 FiLM-based Latent Adaptation

We parameterize batch-specific adaptation using a shared FiLM adapter with batch-indexed parameters (γ_b and β_b). For each batch b , we associate a scale vector $\gamma_b \in \mathbb{R}^d$ and a shift vector $\beta_b \in \mathbb{R}^d$. The adapted embedding is defined as

$$\tilde{z} = \gamma_b \odot z + \beta_b,$$

where \odot denotes element-wise multiplication.

All FiLM parameters are stored in a single shared adapter, implemented as embedding tables indexed by batch identity. This design enables batch-specific modulation while maintaining a unified parameter space suitable for federated aggregation.

3.3 Local Objective with Proximal Regularization

We note that cross-batch alignment in `scBatchProx` does not arise from the local reconstruction objective alone, but from the interaction between shared parameterization, federated aggregation, and proximal regularization across batches.

Each client performs local optimization over its batch-indexed FiLM parameters while starting from the current global adapter state. Given a batch b , the local objective is

$$\begin{aligned} \mathcal{L}_b = & \mathbb{E}_{z \sim Z_b} [\|\gamma_b \odot z + \beta_b - z\|_2^2] \\ & + \mu \left(\|\gamma_b - \gamma_b^{(t)}\|_2^2 + \|\beta_b - \beta_b^{(t)}\|_2^2 \right) \\ & + \lambda (\|\gamma\|_2^2 + \|\beta\|_2^2). \end{aligned}$$

Here, γ_b and β_b denote the batch-specific FiLM parameters for batch b , while γ and β collectively denote all FiLM parameters across batches. The superscript (t) indicates the global adapter parameters at the start of the current federated round. The coefficient μ controls the strength of the FedProx proximal regularization,

and λ controls the ℓ_2 regularization on the adapter weights. For a given batch b , the proximal term is applied only to its corresponding batch-indexed parameters (γ_b, β_b) , while parameters associated with other batches are held fixed during local optimization.

The first term enforces latent consistency by encouraging the adapted embedding to remain close to the original embedding, thereby preventing overcorrection and preserving the geometry induced by the upstream representation while still allowing batch-specific shifts. The proximal term constrains local updates to stay close to the global model, stabilizing optimization under heterogeneous batch distributions. While the latent consistency term preserves upstream geometry, cross-batch alignment is driven by shared parameterization and federated aggregation.

3.4 Federated Optimization Procedure

Training proceeds in rounds. At each round, the server broadcasts the current global FiLM adapter to all clients. Each client performs several epochs of local optimization using its batch-specific data and the objective above. After local training, clients send their updated FiLM parameters to the server.

The server aggregates parameters using weighted federated averaging,

$$\theta^{(t+1)} = \frac{1}{\sum_b n_b} \sum_{b=1}^B n_b \theta_b^{(t+1)},$$

where n_b is the number of samples in batch b . The aggregated parameters define the new global adapter, which is synchronized back to all clients for the next round.

This procedure iteratively refines batch-specific FiLM weights while maintaining a shared global reference, enabling effective batch alignment without centralized data access. Through repeated aggregation, information about shared biological structure is propagated across batches via the global adapter, allowing batch-specific corrections to align embeddings across batches even though optimization is performed locally. Intuitively, `scBatchProx` aligns batches not by directly matching cells across batches, but by enforcing agreement among batch-specific corrections through a shared latent adapter.

3.5 Inference and Post-hoc Integration

After training, the learned FiLM adapter is applied once to the full embedding matrix. Given Z and batch labels $\{b_i\}$, the final batch-corrected embedding is

$$\tilde{Z} = \{\gamma_{b_i} \odot z_i + \beta_{b_i}\}_{i=1}^N.$$

The resulting embedding can be directly used for downstream analysis, visualization, or clustering, and remains compatible with any method that consumes latent representations.

4 Experiments

We now present empirical results for `scBatchProx` by performing all optimization as a lightweight post-hoc stage on top of upstream single-cell embeddings. Given an embedding matrix $Z \in \mathbb{R}^{N \times d}$ and corresponding batch labels, we instantiate a FiLM style latent adapter and optimize only its batch-indexed parameters in a FL-inspired setting, treating each batch as a separate client. On each batch, local training is performed using Adam [3] with learning rate 10^{-3} for two local epochs per federated round. Training proceeds for seven federated rounds by default. Each local objective includes a FedProx proximal penalty with $\mu = 10^{-3}$ and an ℓ_2 regularization term on the adapter embeddings with coefficient $\lambda = 10^{-3}$. We use a batch size of 256 and a fixed 90 percent training split that is reused across all communication rounds to ensure consistent client sampling. Unless otherwise stated, all `scBatchProx` experiments are run on CPU.

4.1 Benchmark

4.1.1 Datasets and Preprocessing

Batch effects in scRNA-seq data arise from two primary sources: within-study technical variation across experimental batches, often reflecting repeated measurements or processing runs within a single study (*multi-batch heterogeneity*), and between-study variation arising from independently designed and executed studies, which may differ in protocols, platforms, or laboratories (*cross-study heterogeneity*). We use a two-batch peripheral blood mononuclear cell (PBMC) dataset to exemplify the former scenario. To evaluate cross-study heterogeneity, we consider the Human Pancreas Multi-Study (HPMS) dataset. For both case studies, we project the data into a low-dimensional UMAP [9] space (Figure 6 in Appendix A) to visualize the original two-dimensional representations with respect to batch or study labels and corresponding cell types. Figure 6 illustrates the extent to which both multi-batch and cross-study heterogeneity distort the underlying biological structure.

For the two-batch PBMC dataset, we exclude cells that contain fewer than 200 detected genes or more than five percent mitochondrial transcript abundance. After removing low-quality cells, we retain genes only if they appear in at least five cells and had a minimum of 500 total counts. We remove ribosomal protein genes to reduce technical noise. We then select 2,500 highly variable genes and

perform data normalization using Scanpy [19] by scaling each cell’s read counts to 10,000 followed by a \log_{1p} transformation. For the HPMS dataset, we adopt the preprocessed version¹ used by scVI, scANVI, and many prior works, in which gene filtering and highly variable gene selection were performed already. Accordingly, we apply only data normalization and a \log_{1p} transformation, following the same procedure as above. Summary statistics for both datasets after preprocessing are reported in Table 2 of Appendix A.

4.1.2 Metrics

We evaluate integration performance using scIB [7], a standardized benchmarking toolkit that quantifies the trade-off between batch-effect removal and biological signal preservation. Biological conservation is assessed using metrics that capture cell-type structure and label agreement, including normalized mutual information (NMI) and adjusted Rand index (ARI) based on K-means clustering, label average silhouette width (ASW), isolated-label F1, and cell-type local inverse Simpson’s index (cLISI). Batch-effect removal is evaluated using complementary metrics that measure batch mixing and dataset alignment, including batch ASW, integration local inverse Simpson’s index (iLISI), kBET per label, graph connectivity, and PCR-based batch association. Together, these metrics provide a comprehensive view of how effectively an integration method removes batch effects while preserving biologically meaningful variation. Full metric definitions and aggregation procedures are provided in Appendix B.

4.1.3 Baselines

We demonstrate the efficacy of scBatchProx on embeddings produced by a set of widely used batch correction and representation learning methods that represent both batch-agnostic and batch-aware approaches. Batch-agnostic baselines include PCA, ICA, and FA, which do not require batch information and are commonly used for exploratory analysis and visualization. For these methods, we fix the latent dimensionality to 40. Batch-aware baselines include scVI, scANVI, and LDVAE, which explicitly incorporate batch labels during model training or alignment. scANVI additionally requires the cell type labels. All baseline methods are run using default settings from their respective implementations, and evaluation is performed on the resulting latent embeddings. For fair comparison, all methods are assessed using the same preprocessing pipeline, evaluation metrics, and scIB configuration.

¹https://docs.scarches.org/en/latest/scvi_surgery_pipeline.html

4.2 Results

4.2.1 Comparison with Baselines

Table 1: Batch correction, biological conservation, aggregate scores, and added runtime overhead (in seconds) across datasets. **Bold** indicates better performance within each data–method pair. All reported runtimes for `scBatchProx` are measured on CPU. `scBatchProx` consistently improves overall embedding quality (Aggregate), primarily through gains in batch correction, while incurring minimal additional runtime (typically around approximately 5 seconds or less).

Data	Method	Batch correction	Bio. conservation	Aggregate	Added Time
Two-batch PBMC	PCA	0.3262	0.6601	0.5266	–
	PCA- <code>scBatchProx</code>	0.3266	0.6603	0.5268	6.05
	ICA	0.5315	0.6706	0.6150	–
	ICA- <code>scBatchProx</code>	0.5328	0.6703	0.6153	6.13
	FA	0.5095	0.6558	0.5973	–
	FA- <code>scBatchProx</code>	0.5103	0.6788	0.6114	3.05
	scVI	0.8047	0.7239	0.7562	–
	scVI- <code>scBatchProx</code>	0.8280	0.7246	0.7660	5.05
	LDVAE	0.6150	0.7331	0.6859	–
	LDVAE- <code>scBatchProx</code>	0.6475	0.7305	0.6973	2.63
	scANVI	0.8269	0.7359	0.7723	–
	scANVI- <code>scBatchProx</code>	0.8426	0.7344	0.7777	2.94
HPMS	PCA	0.3087	0.6473	0.5119	–
	PCA- <code>scBatchProx</code>	0.3087	0.6522	0.5148	3.33
	ICA	0.3433	0.6056	0.5007	–
	ICA- <code>scBatchProx</code>	0.3440	0.6411	0.5223	2.93
	FA	0.3074	0.6168	0.4930	–
	FA- <code>scBatchProx</code>	0.3074	0.6169	0.4931	3.75
	scVI	0.5447	0.6955	0.6352	–
	scVI- <code>scBatchProx</code>	0.5456	0.6965	0.6361	3.59
	LDVAE	0.5027	0.7091	0.6265	–
	LDVAE- <code>scBatchProx</code>	0.5069	0.7095	0.6285	2.59
	scANVI	0.5518	0.7320	0.6599	–
	scANVI- <code>scBatchProx</code>	0.5566	0.7329	0.6624	3.92

Table 1 shows that `scBatchProx` consistently improves aggregate integration scores under both multi-batch and cross-study heterogeneity, with strong gains in batch correction for both linear and deep representations. Moreover, the additional computational overhead introduced by `scBatchProx` is modest relative to the baseline models.

A consistent trend across both datasets is that `scBatchProx` achieves larger relative improvements in batch correction than in biological conservation. This reflects the interaction between the FL-driven optimization strategy and the nature of batch effects. In our formulation, each batch or study is optimized separately, which naturally emphasizes the removal of batch-specific technical variation, while updates are constrained to remain close to a shared reference to prevent incompatible drift. As a result, batch effects, which are inherently local to individual batches,

are effectively reduced. In contrast, preserving biological structure often requires information shared across all batches. Biological signals such as cell-type identity and developmental state are globally defined and may not be fully observable within any single batch. While `scBatchProx` supports strong local alignment, the constraint that keeps batch-specific adjustments aligned across batches limits how much fine-grained biological variation can be modified at the batch level. Consequently, improvements in biological conservation are typically more modest, especially for methods that already encode strong biological priors.

The improvement pattern is particularly pronounced on the HPMS dataset. This is consistent with prior observations in FedProx [5], where proximal regularization is most effective under strong distributional heterogeneity, where data distributions differ substantially across sources. Together, these results highlight a fundamental asymmetry between batch effects, which are primarily local and batch-specific, and biological structure, which is intrinsically global.

4.2.2 Cumulative Retraining Under Dataset Evolution

We simulate cumulative retraining under dataset evolution, where newly sequenced biological samples are combined with all existing data and jointly embedded from scratch using a batch correction method (PCA in this case), followed by post-hoc refinement with `scBatchProx`. Using HPMS, we consider two protocol sequences on HPMS: a realistic progression from droplet-based to plate-based protocols, and the reverse order, which introduces more abrupt changes in protocol composition and dataset scale.

At each cumulative retraining stage, we assess integration quality using `scIB` metrics that remain well defined under sequential dataset expansion with repeated global re-embedding. Specifically, we report K-means NMI and ARI, Leiden NMI and ARI, and ASW scores for biological conservation, together with `iLISI` and ASW scores for batch correction. Metrics that rely on fixed embedding coordinates or stable neighborhood structure across stages are omitted, as their assumptions are violated under cumulative retraining by construction.

As shown in Figure 3, `scBatchProx` consistently improves aggregate integration quality over PCA across both protocol arrival orders throughout cumulative dataset growth.

4.2.3 Continual Training Under Dataset Evolution

In addition to cumulative retraining, we consider a continual integration setting in which the model is not retrained on the full dataset as new data arrive. This setting reflects practical scenarios where repeated global retraining is impractical due to

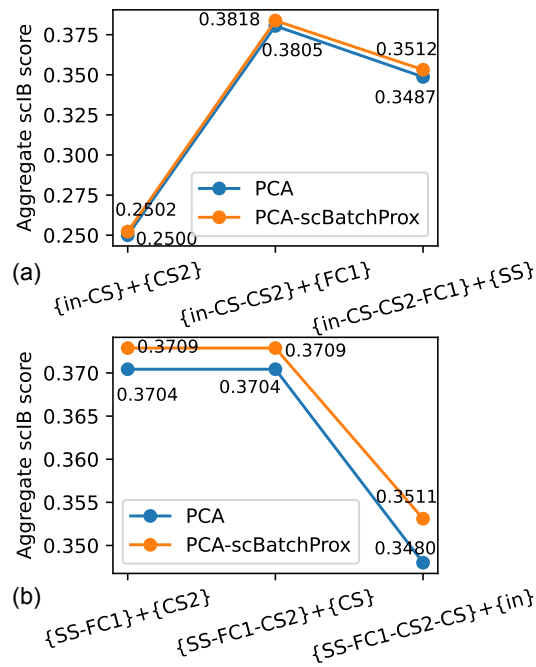


Figure 3: Aggregate scIB scores for cumulative retraining under protocol arrival: (a) technological progression order (inDrop → CEL-Seq → CEL-Seq2 → Fluidigm C1 → Smart-seq2) and (b) reverse order (Smart-seq2 → Fluidigm C1 → CEL-Seq2 → CEL-Seq → inDrop). While cumulative retraining is supported by most existing methods, it is computationally expensive. `scBatchProx` consistently improves overall embedding quality across both arrival orders.

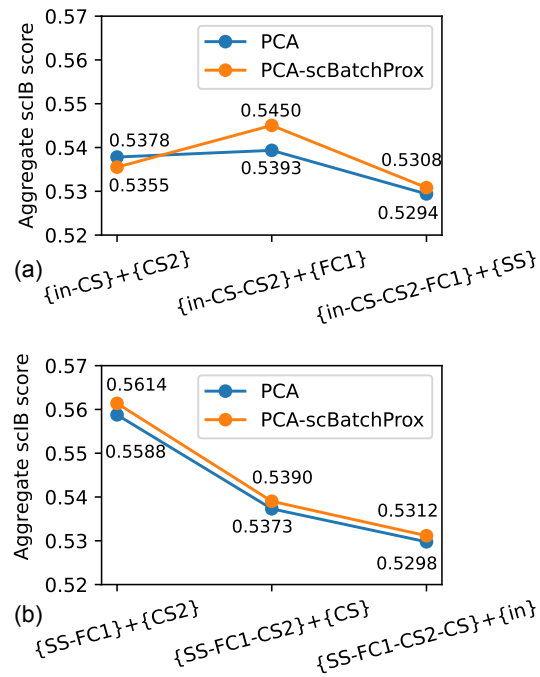


Figure 4: Aggregate scIB scores for continual training under protocol arrival: (a) technological progression order (inDrop → CEL-Seq → CEL-Seq2 → Fluidigm C1 → Smart-seq2) and (b) reverse order (Smart-seq2 → Fluidigm C1 → CEL-Seq2 → CEL-Seq → inDrop). Continual training is commonly encountered in practice, yet most end-to-end batch-aware models do not support it. Despite this constraint, scBatchProx improves embedding quality across both arrival orders.

computational constraints or data scale, such as maintaining a reference atlas that is periodically extended with new studies. In this workflow, an initial reference embedding is constructed using the earliest protocols, and subsequent datasets are integrated by fitting the pretrained integration model only on the newly arrived embeddings. With `scBatchProx`, previously embedded cells retain fixed coordinates, and only batch-specific refinement parameters are updated to accommodate newly arriving batches, thereby preserving the geometry of previously embedded data. Figure 4 shows that `scBatchProx` remains effective under continual training.

4.2.4 Ablation Study

We ablate the proximal term by setting the coefficient to $\mu = 0.0$, removing the constraint that anchors batch-specific updates to the global adapter. In this setting, batch-wise updates are driven solely by local objectives and aggregated without regularization, resulting in unconstrained adaptation.

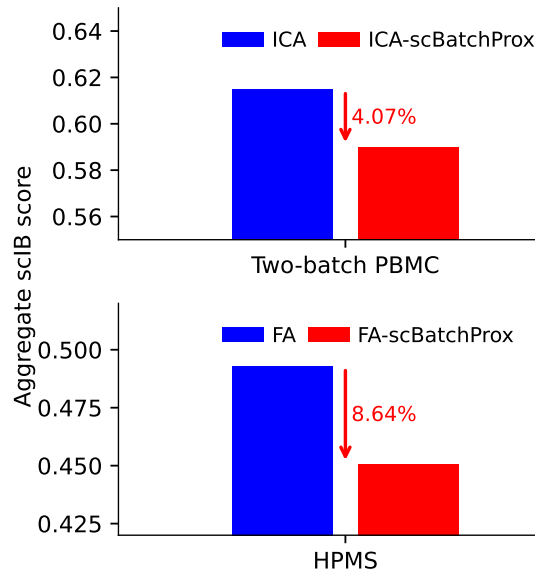


Figure 5: Ablations on 2-batch PBMC (top) and HPMS (bottom) with the proximal coefficient set to $\mu = 0.0$ (no proximal regularization). Complete ablation results are provided in Appendix C. Removing proximal regularization degrades overall performance, primarily due to reduced biological conservation.

Figure 5 and Appendix C report aggregate scores across both datasets. Without proximal regularization, `scBatchProx` exhibits inconsistent performance across

base models and datasets: while some representations improve, others degrade, particularly in biological conservation. This effect is most pronounced for linear methods such as ICA and FA, where unconstrained batch-specific FiLM updates overfit local structure and disrupt shared biological signals.

These results emphasize the importance of proximal regularization in balancing batch-effect removal with preservation of global biological structure. By anchoring batch-specific updates to a shared reference, the proximal term stabilizes optimization under heterogeneous batches and limits incompatible drift, which is especially important in cross-study settings. Overall, this ablation confirms that proximal regularization is a core component of `scBatchProx`, enabling stable and consistent post-hoc refinement across diverse base models and data regimes.

5 Conclusion

We have introduced `scBatchProx`, a post-hoc, FL-inspired optimization framework for refining precomputed single-cell embeddings to correct batch effects in distributed and evolving settings. By operating directly in latent space and optimizing only lightweight batch-conditioned adapters, `scBatchProx` achieves effective batch correction without access to raw data or costly end-to-end retraining. This capability enables the practical reuse and continual refinement of single-cell embeddings as datasets grow and evolve, addressing a fundamental mismatch between existing batch correction methods and how scRNA-seq data are generated, processed, and reused in practice.

References

- [1] Maayan Baron, Adrian Veres, Samuel L. Wolock, Aubrey L. Faust, Renaud Gaujoux, Amedeo Vetere, Jennifer Hyoje Ryu, Bridget K Wagner, Shai S. Shen-Orr, Allon M. Klein, Douglas A. Melton, and Itai Yanai. A single-cell transcriptomic map of the human and mouse pancreas reveals inter- and intra-cell population structure. *Cell Systems*, 3(4):346–360.e4, 2016.
- [2] Paul Datlinger, André F Rendeiro, Thorina Boenke, Martin Senekowitsch, Thomas Krausgruber, Daniele Barreca, and Christoph Bock. Ultra-high-throughput single-cell RNA sequencing and perturbation screening with combinatorial fluidic indexing. *Nature Methods*, 18(6):635–642, 2021.
- [3] Diederik P. Kingma and Jimmy Ba. Adam: A Method for Stochastic Optimization. In *3rd International Conference on Learning Representations, ICLR 2015*, San Diego, CA, USA, 2015.

- [4] Allon M. Klein, Linas Mazutis, Ilke Akartuna, Naren Tallapragada, Adrian Veres, Victor Li, Leonid Peshkin, David A. Weitz, and Marc W. Kirschner. Droplet barcoding for single-cell transcriptomics applied to embryonic stem cells. *Cell*, 161(5):1187–1201, 2015.
- [5] Tian Li, Anit Kumar Sahu, Manzil Zaheer, Maziar Sanjabi, Ameet Talwalkar, and Virginia Smith. Federated optimization in heterogeneous networks. In *Proceedings of Machine Learning and Systems*, volume 2, pages 429–450, Austin, TX, USA, 2020. mlsys.org.
- [6] Romain Lopez, Jeffrey Regier, Michael B. Cole, Michael I. Jordan, and Nir Yosef. Deep generative modeling for single-cell transcriptomics. *Nature Methods*, 15:1053–1058, 2018.
- [7] Malte D Luecken, Maren Büttner, Kridsakorn Chaichoompu, Anna Danese, Marta Interlandi, Michaela F Müller, Daniel C Strobl, Luke Zappia, Martin Dugas, Maria Colomé-Tatché, and Fabian J. Theis. Benchmarking atlas-level data integration in single-cell genomics. *Nature Methods*, 19:41–50, 2022.
- [8] Evan Z. Macosko, Anindita Basu, Rahul Satija, James Nemesh, Karthik Shekhar, Melissa Goldman, Itay Tirosh, Allison R Bialas, Nolan Kamitaki, Emily M. Martersteck, John J. Trombetta, David A. Weitz, Joshua R. Sanes, Alex K. Shalek, Aviv Regev, and Steven A. McCarroll. Highly parallel genome-wide expression profiling of individual cells using nanoliter droplets. *Cell*, 161(5):1202–1214, 2015.
- [9] Leland McInnes, John Healy, and James Melville. Umap: Uniform manifold approximation and projection for dimension reduction. *Journal of Open Source Software*, 3(29):861, 2018.
- [10] H. Brendan McMahan, Eider Moore, Daniel Ramage, Seth Hampson, and Blaise Agüera y Arcas. Communication-efficient learning of deep networks from decentralized data. In *Proceedings of the 20th International Conference on Artificial Intelligence and Statistics*, volume 54, pages 1273–1282, Florida, USA, 2017. Proceedings of Machine Learning Research.
- [11] Mauro J. Muraro, Gitanjali Dharmadhikari, Dominic Grün, Nathalie Groen, Tim Dielen, Erik Jansen, Leon van Gurp, Marten A. Engelse, Françoise Carlotti, Eelco J.P. de Koning, and Alexander van Oudenaarden. A single-cell transcriptome atlas of the human pancreas. *Cell Systems*, 3(4):385–394.e3, 2016.

- [12] Ethan Perez, Florian Strub, Harm De Vries, Vincent Dumoulin, and Aaron Courville. Film: Visual reasoning with a general conditioning layer. In *Proceedings of the Thirty-Second AAAI Conference on Artificial Intelligence and Thirtieth Innovative Applications of Artificial Intelligence Conference and Eighth AAAI Symposium on Educational Advances in Artificial Intelligence*, volume 32, pages 3942–3951, New Orleans, Louisiana, USA, 2018. AAAI Press.
- [13] CZI Cell Science Program, Shibla Abdulla, Brian Aeevermann, Pedro Assis, Seve Badajoz, Sidney M. Bell, Emanuele Bezzi, Batuhan Cakir, Jim Chaffer, Signe Chambers, J Michael Cherry, Tiffany Chi, Jennifer Chien, Leah Dorman, Pablo Garcia-Nieto, Nayib Gloria, Mim Hastie, Daniel Hegeman, Jason Hilton, Timmy Huang, Amanda Infeld, Ana-Maria Istrate, Ivana Jelic, Kuni Katsuya, Yang Joon Kim, Karen Liang, Mike Lin, Maximilian Lombardo, Bailey Marshall, Bruce Martin, Fran McDade, Colin Megill, Nikhil Patel, Alexander Predeus, Brian Raymor, Behnam Robatmili, Dave Rogers, Erica Rutherford, Dana Sadgat, Andrew Shin, Corinn Small, Trent Smith, Prathap Sridharan, Alexander Tarashansky, Norbert Tavares, Harley Thomas, Andrew Tolopko, Meghan Urisko, Joyce Yan, Garabet Yeretssian, Jennifer Zamanian, Arathi Mani, Jonah Cool, and Ambrose Carr. CZ CELLxGENE Discover: a single-cell data platform for scalable exploration, analysis and modeling of aggregated data. *Nucleic Acids Research*, 53(D1):D886–D900, 2025.
- [14] Aviv Regev, Sarah A. Teichmann, Eric S. Lander, Ido Amit, Christophe Benoist, Ewan Birney, Bernd Bodenmiller, Peter Campbell, Piero Carninci, Menna Clatworthy, Hans Clevers, Bart Deplancke, Ian Dunham, James Eberwine, Roland Eils, Wolfgang Enard, Andrew Farmer, Lars Fugger, Berthold Göttgens, Nir Hacohen, Muzlifah Haniffa, Martin Hemberg, Seung Kim, Paul Klenerman, Arnold Kriegstein, Ed Lein, Sten Linnarsson, Emma Lundberg, Joakim Lundeberg, Partha Majumder, John C. Marioni, Miriam Merad, Musa Mhlanga, Martijn Nawijn, Mihai Netea, Garry Nolan, Dana Pe’er, Anthony Phillipakis, Chris P. Ponting, Stephen Quake, Wolf Reik, Orit Rozenblatt-Rosen, Joshua Sanes, Rahul Satija, Ton N Schumacher, Alex Shalek, Ehud Shapiro, Padmanee Sharma, Jay W. Shin, Oliver Stegle, Michael Stratton, Michael J. T. Stubbington, Fabian J. Theis, Matthias Uhlen, Alexander van Oudenaarden, Allon Wagner, Fiona Watt, Jonathan Weissman, Barbara Wold, Ramnik Xavier, Nir Yosef, and Human Cell Atlas Meeting Participants. The human cell atlas. *eLife*, 6:e27041, 2017.
- [15] Ansuman T. Satpathy, Jeffrey M. Granja, Kathryn E. Yost, Yanyan Qi, Francesca Meschi, Geoffrey P. McDermott, Brett N. Olsen, Maxwell R. Mum-

- bach, Sarah E. Pierce, M. Ryan Corces, Preyas Shah, Jason C. Bell, Darisha Jhutti, Corey M. Nemece, Jean Wang, Li Wang, Yifeng Yin, Paul G. Giresi, Anne Lynn S. Chang, Grace X. Y. Zheng, William J. Greenleaf, and Howard Y. Chang. Massively parallel single-cell chromatin landscapes of human immune cell development and intratumoral T cell exhaustion. *Nature Biotechnology*, 37:925–936, 2019.
- [16] Åsa Segerstolpe, Athanasia Palasantza, Pernilla Eliasson, Eva-Marie Andersson, Anne-Christine Andréasson, Xiaoyan Sun, Simone Picelli, Alan Sabirsh, Maryam Clausen, Magnus K Bjursell, David M. Smith, Maria Kasper, Carina Ämmälä, and Rickard Sandberg. Single-cell transcriptome profiling of human pancreatic islets in health and type 2 diabetes. *Cell Metabolism*, 24(4):593–607, 2016.
- [17] Valentine Svensson, Adam Gayoso, Nir Yosef, and Lior Pachter. Interpretable factor models of single-cell RNA-seq via variational autoencoders. *Bioinformatics*, 36(11):3418–3421, 2020.
- [18] Yue J. Wang, Jonathan Schug, Kyoung-Jae Won, Chengyang Liu, Ali Naji, Dana Avrahami, Maria L. Golson, and Klaus H. Kaestner. Single-cell transcriptomics of the human endocrine pancreas. *Diabetes*, 65(10):3028–3038, 2016.
- [19] F. Alexander Wolf, Philipp Angerer, and Fabian J. Theis. SCANPY: large-scale single-cell gene expression data analysis. *Genome Biology*, 19:15, 2018.
- [20] Yurong Xin, Jinrang Kim, Haruka Okamoto, Min Ni, Yi Wei, Christina Adler, Andrew J. Murphy, George D. Yancopoulos, Calvin Lin, and Jesper Gromada. RNA sequencing of single human islet cells reveals type 2 diabetes genes. *Cell Metabolism*, 24(4):608–615, 2016.
- [21] Chenling Xu, Romain Lopez, Edouard Mehlman, Jeffrey Regier, Michael I Jordan, and Nir Yosef. Probabilistic harmonization and annotation of single-cell transcriptomics data with deep generative models. *Molecular Systems Biology*, 17:MSB20209620, 2021.
- [22] Grace X. Y. Zheng, Jessica M. Terry, Phillip Belgrader, Paul Ryvkin, Zachary W. Bent, Ryan Wilson, Solongo B. Ziraldo, Tobias D. Wheeler, Geoff P. McDermott, Junjie Zhu, Mark T. Gregory, Joe Shuga, Luz Montesclaros, Jason G. Underwood, Donald A. Masquelier, Stefanie Y. Nishimura, Michael Schnall-Levin, Paul W. Wyatt, Christopher M. Hindson, Rajiv Bharadwaj, Alexander Wong, Kevin D. Ness, Lan W. Beppu, H. Joachim Deeg, Christopher McFarland, Keith R. Loeb, William J. Valente, Nolan G. Ericson, Emily A.

Stevens, Jerald P. Radich, Tarjei S. Mikkelsen, Benjamin J. Hindson, and Jason H. Bielas. Massively parallel digital transcriptional profiling of single cells. *Nature Communications*, 8:14049, 2017.

Appendix

A SUMMARY OF PREPROCESSED DATASETS

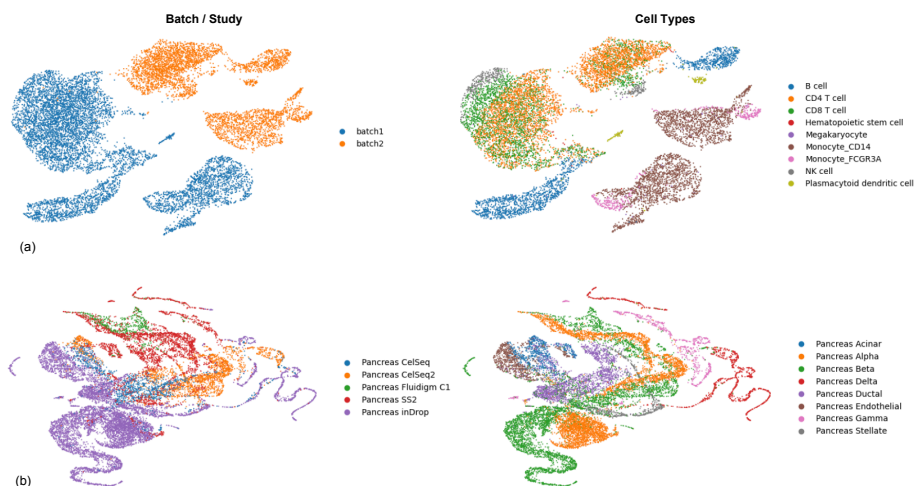


Figure 6: UMAP visualizations of the original representations for (a) the two-batch PBMC dataset and (b) the HPMS dataset. Technical variation is clearly visible in both cases. For example, CD4 T cells in the two-batch PBMC dataset separate primarily by batch rather than forming a coherent biological cluster.

Table 2: Summary statistics of the datasets used after data preprocessing

Data	Tissue	Batch/Study	Cells	Genes	Cell Types
Two-batch PBMC	Blood	2 batches with different chemistries: 3'–5' and 5'–3' [22]	12,013	2,500	9
HPMS	Pancreas	5 protocol-specific studies: CEL-Seq, CEL-Seq2, Smart-seq2, Fluidigm C1, and inDrop [1, 11, 16, 18, 20]	15,681	1,000	8

B METRICS – DEFINITIONS AND INTERPRETATION

We evaluate data integration performance using the scIB benchmarking framework [7], which provides a standardized collection of quantitative metrics to assess the trade-off between batch-effect removal and biological signal preservation. All metrics are computed on the low-dimensional integrated representations produced by each method unless stated otherwise.

B.1 Biological Conservation Metrics

Biological conservation metrics quantify how well biologically meaningful structure, in particular cell-type identity and local neighborhood relationships, is preserved after integration.

Clustering-based label agreement (NMI, ARI). We assess global agreement between unsupervised clustering results and ground-truth cell-type annotations using normalized mutual information (NMI) and adjusted Rand index (ARI). Let C denote the clustering assignment obtained by applying K-means to the integrated embedding and Y the true cell-type labels. NMI is defined as

$$\text{NMI}(C, Y) = \frac{2I(C; Y)}{H(C) + H(Y)},$$

where $I(\cdot; \cdot)$ denotes mutual information and $H(\cdot)$ denotes entropy. ARI measures pairwise agreement between C and Y , adjusted for chance, with values closer to 1 indicating better recovery of cell-type structure.

Cell-type average silhouette width (ASW). The silhouette width for a cell i is defined as

$$s(i) = \frac{b(i) - a(i)}{\max\{a(i), b(i)\}},$$

where $a(i)$ is the average distance from i to other cells of the same cell type and $b(i)$ is the minimum average distance to cells of a different cell type. The cell-type ASW is computed by averaging $s(i)$ across all cells and rescaled to $[0, 1]$ as

$$\text{ASW}_{\text{cell}} = \frac{\text{ASW} + 1}{2},$$

with higher values indicating better separation between cell types.

Isolated-label F1 score. The isolated-label F1 score evaluates preservation of rare or batch-specific cell types that appear in only a subset of batches. For each isolated label, precision and recall are computed based on neighborhood consistency, and the F1 score is defined as

$$\text{F1} = \frac{2 \cdot \text{precision} \cdot \text{recall}}{\text{precision} + \text{recall}}.$$

Higher values indicate improved conservation of rare cell populations.

Cell-type local inverse Simpson’s index (cLISI). cLISI measures the diversity of cell-type labels within local neighborhoods of the integrated embedding. For a cell i , cLISI is defined as

$$\text{cLISI}(i) = \left(\sum_c p_{i,c}^2 \right)^{-1},$$

where $p_{i,c}$ denotes the proportion of neighbors of i belonging to cell type c . Lower cLISI values indicate stronger local cell-type purity and better biological conservation.

B.2 Batch-Effect Removal Metrics

Batch-effect removal metrics quantify how effectively technical variation across batches or datasets is mitigated while avoiding overcorrection.

Batch average silhouette width (batch ASW). Batch ASW is computed analogously to cell-type ASW, but using batch labels instead of cell-type labels. For each cell i , the absolute silhouette width $|s(i)|$ is computed and rescaled such that

$$\text{ASW}_{\text{batch}} = 1 - |s(i)|.$$

Higher values indicate better batch mixing.

Integration local inverse Simpson’s index (iLISI). iLISI evaluates batch diversity within local neighborhoods. For a cell i ,

$$\text{iLISI}(i) = \left(\sum_b p_{i,b}^2 \right)^{-1},$$

where $p_{i,b}$ denotes the proportion of neighbors from batch b . Higher iLISI values indicate stronger batch mixing.

kBET per label. The k-nearest neighbor batch effect test (kBET) evaluates whether batch labels are uniformly distributed within local neighborhoods. In the per-label variant, kBET is applied separately within each cell type. The final score is the average acceptance rate across labels, with higher values indicating reduced batch effects.

Graph connectivity. Graph connectivity measures whether cells of the same cell type form a connected component across batches in a k-nearest neighbor graph constructed on the integrated representation. Let G_c denote the subgraph induced by cells of cell type c . The connectivity score is defined as the fraction of nodes belonging to the largest connected component of G_c , averaged across cell types. Higher values indicate successful integration without fragmenting biological structure.

Principal component regression (PCR). PCR quantifies the fraction of variance in the integrated embedding explained by batch labels. Let Z denote the integrated representation and S the batch labels. PCR is computed by regressing principal components of Z on S , and the coefficient of determination R^2 is averaged across components. Lower PCR values indicate reduced batch-associated variance.

B.3 Aggregate Scores

To summarize integration performance, scIB aggregates individual metrics into composite scores. All metrics are first scaled to the unit interval $[0, 1]$, with higher values indicating better performance.

The biological conservation score is computed as the arithmetic mean of all biological conservation metrics,

$$\text{Bio} = \frac{1}{|\mathcal{M}_{\text{bio}}|} \sum_{m \in \mathcal{M}_{\text{bio}}} m,$$

where \mathcal{M}_{bio} includes NMI, ARI, cell-type ASW, isolated-label F1, and cLISI.

Similarly, the batch-effect removal score is computed as

$$\text{Batch} = \frac{1}{|\mathcal{M}_{\text{batch}}|} \sum_{m \in \mathcal{M}_{\text{batch}}} m,$$

where $\mathcal{M}_{\text{batch}}$ includes batch ASW, iLISI, kBET per label, graph connectivity, and PCR.

Following scIB conventions, the overall integration score is computed as a weighted mean,

$$\text{Overall} = 0.6 \cdot \text{Bio} + 0.4 \cdot \text{Batch},$$

placing greater emphasis on biological conservation while still encouraging effective batch-effect removal.

C COMPLETE COMPARISON TABLES.

Table 3: Batch correction, biological conservation, and aggregate scores across datasets with the proximal coefficient set to $\mu = 0.0$ (no proximal regularization). **Bold** indicates better performance within each method pair.

Dataset	Method	Batch correction	Bio. conservation	Aggregate
Two-batch PBMC	PCA	0.3262	0.6601	0.5266
	PCA-scBatchProx	0.3481	0.6515	0.5301
	ICA	0.5315	0.6706	0.6150
	ICA-scBatchProx	0.5455	0.6198	0.5900
	FA	0.5095	0.6558	0.5973
	FA-scBatchProx	0.5109	0.6803	0.6126
	scVI	0.8047	0.7239	0.7562
	scVI-scBatchProx	0.8221	0.7247	0.7636
	LDVAE	0.6150	0.7331	0.6859
	LDVAE-scBatchProx	0.6484	0.7303	0.6975
	scANVI	0.8269	0.7359	0.7723
	scANVI-scBatchProx	0.8066	0.7536	0.7748
HPMS	PCA	0.3087	0.6473	0.5119
	PCA-scBatchProx	0.3087	0.6522	0.5148
	ICA	0.3433	0.6056	0.5007
	ICA-scBatchProx	0.3740	0.6055	0.5129
	FA	0.3074	0.6168	0.4930
	FA-scBatchProx	0.3090	0.5447	0.4504
	scVI	0.5447	0.6955	0.6352
	scVI-scBatchProx	0.5445	0.6977	0.6364
	LDVAE	0.5027	0.7091	0.6265
	LDVAE-scBatchProx	0.5112	0.7421	0.6497
	scANVI	0.5518	0.7320	0.6599
	scANVI-scBatchProx	0.5504	0.7274	0.6566